NOTE

Derivation of seismic cone interval velocities utilizing forward modeling and the downhill simplex method

Erick J. Baziw

Abstract: The seismic cone penetration test (SCPT) has proven to be a very valuable geotechnical tool in facilitating the determination of low strain ($<10^{-4}$%) in situ compression (P) and shear (S) wave velocities. The P- and S-wave velocities are directly related to the soil elastic constants of Poisson's ratio, shear modulus, bulk modulus, and Young's modulus. The accurate determination of P- and S-wave velocities from the recorded seismic cone time series is of paramount importance to the evaluation of reliable elastic constants. Furthermore, since the shear and compression wave velocities are squared in deriving the elastic constants, small variations in the estimated velocities can cause appreciable errors. The standard techniques implemented in deriving SCPT interval velocities rely upon obtaining reference P- and S-wave arrival times as the probe is advanced into the soil profile. By assuming a straight ray travel path from the source to the SCPT seismic receiver and calculating the relative reference arrival time differences, interval SCPT velocities are obtained. The forward modeling – downhill simplex method (FMDSM) outlined in this paper offers distinct advantages over conventional SCPT velocity profile estimation methods. Some of these advantages consist of the allowance of ray path refraction, greater sophistication in interval velocity determination, incorporation of measurement weights, and meaningful interval velocity accuracy estimators.

Key words: seismic cone penetration testing (SCPT), downhill simplex method (DSM), forward modeling, Fermat's principle, weighted least squares (l_2 norm), cost function.

Résumé : L'essai de pénétration au cône sismique (SCPT) s'est révélé être une outil géotechnique très valable pour faciliter la détermination in situ des vélocités des ondes de compression (P) et de cisaillement (S) à de faibles déformations ($<10^{-4}$ %). Les vélocités de l'onde P et des ondes de cisaillement S sont en relation directe avec les constantes élastiques des sols, soit le rapport de Poisson, le module de cisaillement, le module de masse, et le module de Young. La détermination précise des vélocités des ondes P et S en partant des enregistrements des séries temporelles de cônes sismiques est d'une importance majeure pour l'évaluation fiable des constantes élastiques. De plus, puisque les vélocités des ondes de cisaillement et de compression sont mises au carré dans la dérivation des constantes élastiques, de faibles variations peuvent causer des erreurs appréciables. Les techniques standard introduites dans la dérivation des intervalles de vitesse du SCPT reposent sur l'obtention des temps d'arrivée de référence des ondes P et S alors que la sonde est foncée dans le profil de sol. En supposant un cheminement droit du trajet du rayon de la source au récepteur sismique SCPT et en calculant les différences relatives de temps d'arrivée de référence, on obtient les vélocités des intervalles du SCPT. Le modèle de projection/la méthode simplex (FMDSM) décrits dans cet article offre des avantages par rapport aux méthodes conventionnelles d'estimation du profil de vélocité du SCPT. Certains de ces avantages comprennent la possibilité de réfraction du trajet du rayon, une plus grande sophistication dans la détermination de la vitesse des intervalles, l'incorporation des poids de mesure, et des estimateurs de la vitesse des intervalles d'une précision significative.

Mots clés : essai de pénétration de cône sismique (SCPT), méthode simplex descendante (DSM), modèle de projection, principe de Fermat, ligne des moindres carrés (l_2 norme), fonction de coûts.

[Traduit par la Rédaction]

Received 19 June 2001. Accepted 21 May 2002. Published on the NRC Research Press Web site at http://cgj.nrc.ca on 16 September 2002.

E.J. Baziw. Baziw Consulting Engineers Ltd., 3432 West 23rd Avenue, Vancouver, BC V6S 1K3, Canada (e-mail: staff@bcengineers.com).

 DOI: 10.1139/T02-061

Introduction

Accurate in situ P- and S-wave velocity profiles are essential in geotechnical foundation designs. These parameters are used in both static and dynamic soil analysis where the elastic constants are input variables into the models defining the different states of deformations, such as elastic, elastoplastic, and failure (Finn 1984). Equation [1] illustrates the relationship between the elastic constants of Poisson's ratio (ν), shear modulus (G_0), Young's modulus (E), and bulk modulus (B) with the compression wave velocity (i.e., V_p) and the shear wave velocity (i.e., V_s).

$$\nu = \frac{1 - 2(V_s - V_p)^2}{2 - 2(V_s - V_p)^2}$$

$$G_0 = \rho V_s^2 \qquad [1]$$

$$E = \frac{2\rho V_s^2(2 + \nu)(1 + \nu)}{\nu}$$

$$B = \frac{E}{3(1 - 2\nu)}$$

where ρ is the mass density of the soil. Some static soil analysis techniques include displacements from line loads (i.e., f(E,ν)), one dimensional consolidation settlement (i.e., f(m_v) where $m_v = 1/B$), and soil-structure interaction problems (i.e., f(E,v, B)). The associated methods of response in dynamic soil analysis are the linear method (linear elastic model), the equivalent linear method (visco-elastic model), and the step-by-step integration method (load history tracing). All of the dynamic analysis programs require accurate input parameters for shear modulus, bulk modulus, Young's modulus, and attenuation (i.e., Q value). Dynamic analysis in geotechnical practice is intimately related to the capability of measuring the necessary soil properties.

Another important use of estimated shear wave velocities in geotechnical design is in the liquefaction assessment of soils. As stated by Andrus et al. (1999), "predicting the liquefaction resistance of soil is an important step in the engineering design of new structures and the retrofit of existing structures in earth-quake prone regions." Since the shear wave velocity is influenced by many of the variables that influence liquefaction (i.e., void ratio, soil density, confining stress, stress history, and geologic age), it is an excellent index of liquefaction (Andrus et al. 1999).

The seismic cone has proven to be a very accurate and reliable tool in the determination of V_s and V_p profiles. The advantages of the seismic cone consist of excellent soil probe coupling, a controllable source, and cost effectiveness because it is a retrievable probe. Details of the seismic cone, the downhole test procedures, and comparisons with the crosshole results at several sites have been described by Campanella et al. (1986).

In general terms, the seismic cone is advanced to the depth of interest using a hydraulic reactionary pushing force. An important factor in SCPT is to generate clean and strong source wavelets. In mathematically modeling the displacement responses of a medium to a seismic source, Gibowicz and Kijko (1994) identify the far-field responses as being composed of two terms. The first response is in the direction of the ray path, corresponding to the P-wave motion, and the second response is in a direction perpendicular to the ray path, corresponding to the S-wave motion. The total displacement vector is written as

$$u = u^P + u^S \qquad [2]$$

Gibowicz and Kijko (1994) decompose the u^S displacement into two vectors u^{SV} and u^{SH}, one in a vertical plane that contains the source and the seismic receiver, and the other in a horizontal plane. The relationships are illustrated in Fig. 1.

Seismic sources for engineering investigations are often designed to generate either dominantly P- and SV-waves or dominantly SH-waves due to the fundamentally different behaviour of P-, SV-, and SH-waves at a boundary (Mooney 1977). When a P- or a SV-wave strikes a boundary, four outgoing waves are generated: SV and P, reflected and transmitted. In contrast, a SH wave will only generate reflected and transmitted SH-waves, thus simplifying the recorded seismic time series. A popular SH source is the hammer beam, which consists of applying a hammer blow laterally to the sides of specially designed plates fixed at the surface. The hammer beam generates excellent polarized SH-wavelets and it is standardly applied in reverse polarity analysis (Baziw et al. 1989). Figure 2 illustrates a typical reversely polarized SCPT profile with an 8th order digital bandpass filter applied to the recorded time series.

The reverse polarity technique is the most common method implemented in deriving SCPT interval velocity profiles. Generally, the first or second crossover of the reversely polarized SH-wavelets are selected as the reference arrival times as is illustrated in Fig. 2. The interval velocities are obtained by calculating the relative arrival time differences (e.g., $\Delta T = T_2 - T_1$) and by assuming straight ray travel paths from source to receiver when calculating the travel path differences (i.e., $v = \Delta d/\Delta T$, where Δd is the relative travel path difference and v is the SCPT interval velocity). The reverse polarity technique can be highly susceptible to human bias because it relies on the operator to select a single point that defines the crossover point and subsequent interval time.

Another technique utilized in deriving SCPT interval velocities is based upon cross-correlating the wavelets recorded at consecutive depth increments (Baziw 1993*a*, 1993*b*). The value of the time shift at the maximum crosscorrelation value is assumed to be the relative travel time difference for the wavelet to travel the depth increment. This technique has the following advantages over the reverse polarity technique:

(1) Minimizes the human bias associated with visually selecting a crossover point in deriving interval times, which is required by the reverse polarity technique.

(2) Utilizes the full waveform in deriving interval travel times as opposed to a single point.

(3) The correlation coefficient between the two wavelets can be used as a velocity accuracy estimate. This parameter gives the investigator an indication of the similarity between the two wavelets being correlated and the subsequent accuracy of the velocity estimate.

(4) Obtains two independent velocity estimates for each depth increment by comparing source wavelets generated by

Fig. 1. Decomposition of the S-wave displacement vector u^S into two vectors, u^{SV} and u^{SH}. The three vectors lie in the plane perpendicular to the ray path u^P, and u^{SV} is in the vertical plane, which also contains u^P. The u^S angle of polarization is denoted by ε (after Gibowics and Kijko 1994).

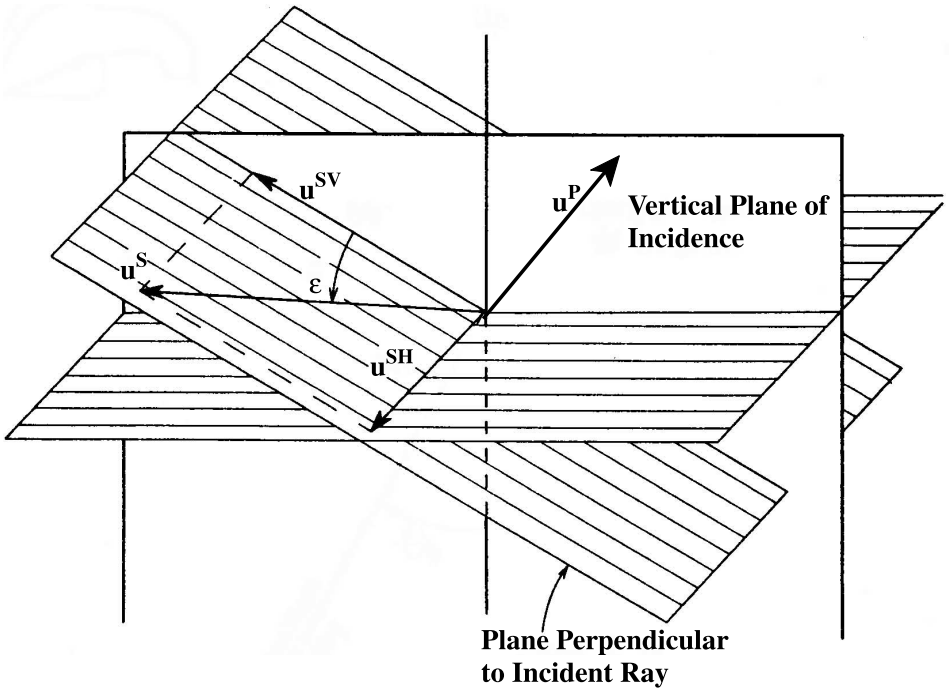

Fig. 2. Typical reversely polarized SCPT profile with an 8th order, zero phase bandpass filter applied to the recorded time series.

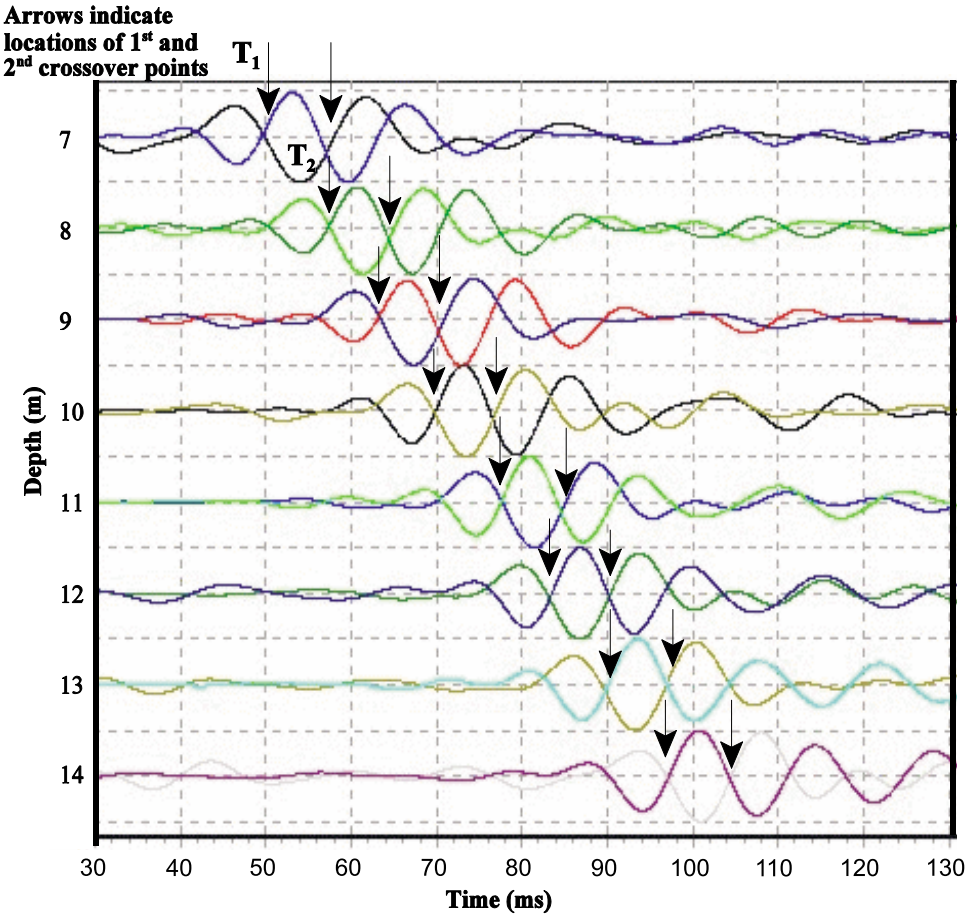

the impacts on both the right and left side of the hammer beam.

Some other SCPT arrival time techniques include the implementation of real-time Kalman filtering techniques (Baziw and Weir-Jones 2002) and the utilization of source wavelet angles of incidence from hodogram analysis in biaxial and triaxial SCPT probe configurations. Hodogram analysis (Kanasewich 1981) allows for full waveform analysis and identification and gives a quantitative indication (i.e., correlation) between *X*-, *Y*-, and *Z*-component SCPT time series.

From the recorded seismic cone time series, arrival times for the S- and P-waves are determined and the corresponding velocity profiles are derived. In all of the previously described SCPT interval velocity estimation techniques, it is mandatory that the SCPT data acquisition system utilized does not introduce spectral smearing or phase shifting into the recorded seismic time series as is illustrated in Fig. 3 (Baziw et al. 2000). This phenomenon may occur if the ambient background noise contains frequency components that exceed the seismic sensor's frequency response limitations.

All of the previously described SCPT interval velocity estimation techniques derive deterministic arrival times and assume straight ray paths between source and receiver. They do not allow for the incorporation of several varying input measurement parameters (eg., crossover times, maximum crosscorrelation time shift, angles of incidence, and P-, S-wave arrival time separation) in estimating interval velocities. In addition, it is difficult to include measurement reliability and (or) accuracy weights into the interval velocity estimation algorithms; there are a limited number of recorded waveforms that can be used in the velocity estimation, a reliable indication of the accuracy of the estimated SCPT interval velocity profile is lacking, and the straight ray path assumption may result in inaccurate interval velocity estimates. The forward modeling – downhill simplex method (FMDSM) outlined in this paper attempts to address some of these limitations.

The FMDSM for SCPT interval velocity estimation

The FMDSM algorithm presented in this section attempts to provide more intelligence in SCPT interval velocity estimations compared to the established techniques previously described. Some of the advantages of the FMDSM are as follows:

(1) The refraction of ray path at layer boundaries is considered using Snell's law.

(2) Extensive SCPT time series measurement information (e.g., arrival times, crosscorrelation time shifts, P-, S-wave time separation, and angles of incidence) is taken into account within an optimizes nonlinear cost function.

(3) The measurement weights are specified.

(4) Up to five independent seismic traces acquired from adjacent depth increments are used when deriving one interval velocity.

(5) There is the possibility of unlimited input data (e.g., crossover point arrival times, maximum crosscorrelation time shifts, angles of incidence, and P-, S-wave time separations) into the interval velocity estimation algorithm.

(6) It allows for variable interval velocity estimates so that comparisons or correlations can be made with other types of in situ measurements.

(7) It provides accurate interpolation of interval velocities when data is not available.

(8) Meaningful error residuals can be determined for the evaluation of the accuracy of the estimated interval velocity.

Downhill simplex method in multidimensions

The downhill simplex method (DSM) is an iterative minimization technique originally developed by Nelder and Mead (1965). The DSM in multidimensions has the important property of not requiring derivatives of function evaluations and it can minimize nonlinear functions of more than one independent variable. Although it is not the most efficient optimization procedure, the DSM is versatile, robust, and simple to implement. The DSM has been used in a variety of scientific applications such as obtaining seismic source locations in the mining and oil and gas industries (Vance et al. 1988; Gibowicz and Kijko 1994).

A simplex defines the most elementary geometric figure of a given dimension: a line in one dimension, the triangle in two dimensions, the tetrahedron in three, etc; therefore, in an *N*-dimensional space, the simplex is a geometric figure that consists of $N + 1$ fully interconnected vertices. For example, in determining the location of a seismic event, a three-dimensional space is searched, so the simplex is a tetrahedron with four vertices as illustrated in Fig. 4. The DSM starts at the $N + 1$ vertices that form the initial simplex. The initial simplex vertices are chosen so that the simplex occupies a good portion of the solution space. In addition, it is also required that a scalar cost function (e.g., root mean square (RMS) difference between synthetic and actual seismic receiver arrival times and crosscorrelation time shifts) be specified at each vertex of the simplex.

The general idea of the minimization is to keep the minimum within the simplex during the optimization; at the same time decreasing the volume of the simplex. The DSM searches for the minimum of the costs function by taking a series of steps, each time moving a point in the simplex away from where the cost function is largest. As illustrated in Fig. 4 for the tetrahedron, the simplex moves in space by variously reflecting, expanding, contracting, or shrinking. The simplex size is continuously changed and mostly diminished, so that finally it is small enough to contain the minimum with the desired accuracy.

The DSM incorporates the following basic steps (Vance et al. 1988):

(1) Specify initial simplex vertices.

(2) Specify the cost function at each vertex of the simplex.

(3) Compare the cost function for each vertex and determine the lowest error "best" and highest error "worst" vertices.

(4) In sequence, locating reflected, then if necessary, expanded, then if necessary, contracted vertices, and calculating for each the corresponding cost function and comparing it to the worst vertex; if at any step the cost function of the new trial point is less than the value at the worst vertex; then this vertex is substituted as a vertex in place of the current worst vertex.

Fig. 3. SCPT data illustrating the time series corrupting effects of spectral smearing and phase shifting.

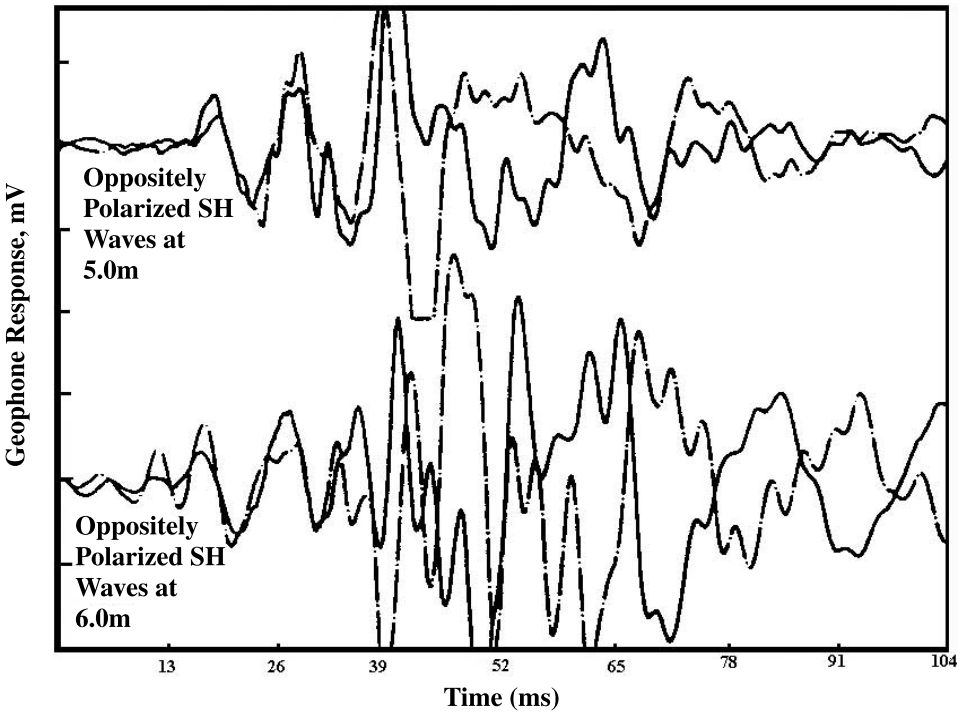

Fig. 4. Initial tetrahedron simplex with possible operations on simplex vertices.

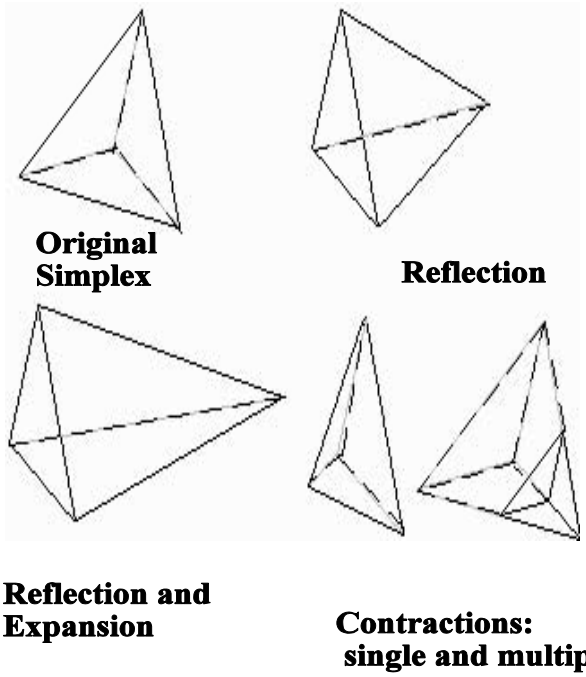

(5) If the process in step (4) does not yield a lower error value than the previous worst, then the other vertices are shrunken towards the best vertex.

(6) At each stage of shrinking, the distances between vertices are calculated and compared to a set tolerance (i.e., *VertexTolerance* variable in the FMDSM algorithm) value to check if the simplex has become sufficiently small for termination of the estimation; when the test criterion is reached, the previous best vertex becomes the solution.

(7) At each stage of shrinking, the cost function values at the vertices is compared to a set minimum (i.e., *CostMinimum* variable in the FMDSM algorithm) value to check if the error residual has become sufficiently small for termination of the estimation; when the test criterion is reached, the previous best vertex becomes the solution.

For the FMDSM algorithm a three-dimensional space is specified, so the simplex is a tetrahedron with four vertices. The FMDSM three-dimensional space consists of three concurrent interval velocities (v_1, v_2, v_3) to be estimated. For simplicity, the cost function presented in this paper is defined as the weighted least squares (l_2 norm) error residual between synthetic and measured arrival times and between synthetic and measured crosscorrelation time shifts for recorded S- and P-waves. More elaborate cost functions, which include the weighted least squares residuals between synthetic angles of incidence, crossover times, P-, S-wave time separations and those measured, may also be used.

The three-dimensional space was selected so that the computational burden was minimized for each FMDSM estimation and so that the complexity of the specification of the initial simplex vertices was reduced. A detailed description of the FMDSM will be provided in a later section.

Forward modelling with Chander's ray tracing technique

As previously described, the DSM requires a cost function to be calculated and minimized while the simplex moves in space by variously reflecting, expanding, contracting, or shrinking. The cost function is derived from the difference between recorded SCPT P- or S-wave arrival and cross-

Fig. 5. Refraction of source wavelet as it travels from source to receiver.

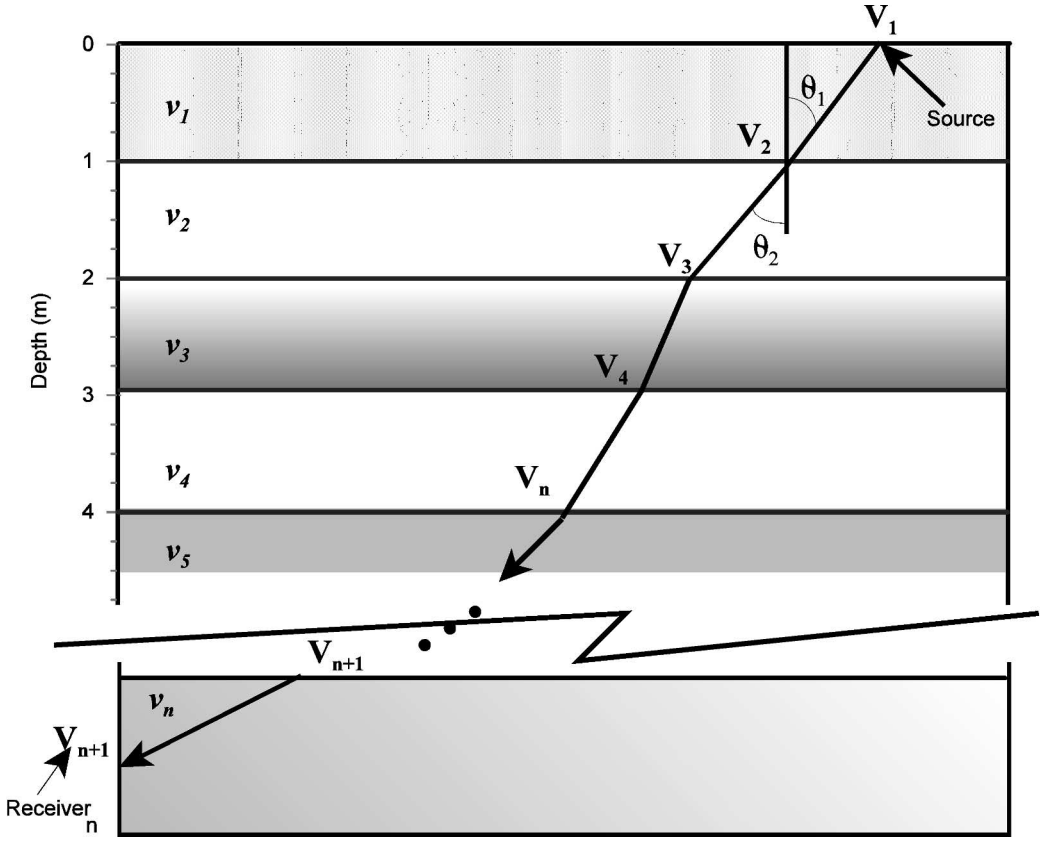

Fig. 6. Example of specification of typical SCPT geometry of stratigraphic profile and probe locations.

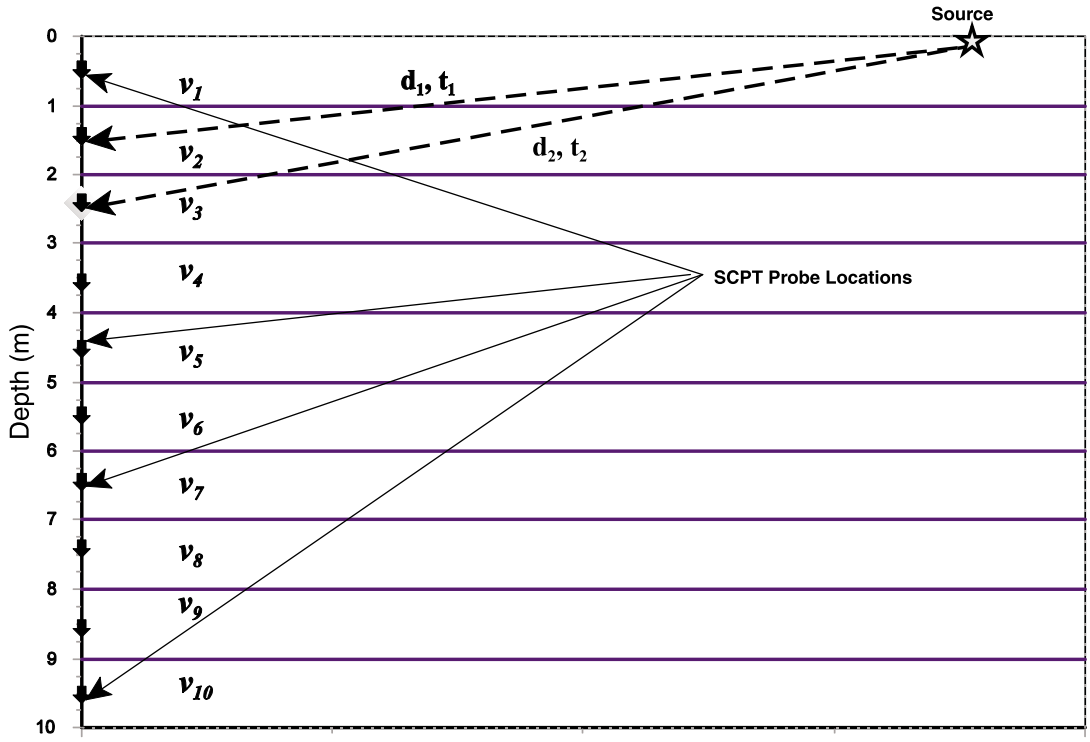

correlation times and those calculated from forward modeling utilizing Chander's ray tracing technique. The FMDSM scalar cost function J for the vertices of the simplex (i.e., i = 1–4) is defined as follows:

$$[3] \qquad J_i = \sum_{k=1}^{N} \sqrt{w_k^{A}[t_k^{Am} - t_k^{As}(v_{1i},\, v_{2i},\, v_{3i})]^2} + \sum_{k=1}^{N-1} \sqrt{w_k^{CC}[t_k^{CCm} - t_k^{CCs}(v_{1i},\, v_{2i},\, v_{3i})]^2}$$

where N defines the number of recorded seismic rays that travel through the three stratigraphic layers (v_1, v_2, and v_3) to be estimated, t^{Am} is the measured seismic wave arrival time with w^{A} representing the weight or accuracy in the range of 0–1, t^{CCm} is the measured crosscorrelation time shift with w^{CC} representing the correlation coefficient or accuracy in the range of 0–1, and t^{As} and t^{CCs} define the synthetic arrival time and crosscorrelation time shift, respectively, derived through forward modeling with Chander's ray tracing technique.

In SCPT the source wavelet travels through the stratigraphic profile and is refracted at layer boundaries. The geometry of the various reflected and refracted waves related to the incident wave is directly analogous to light and can be described, using Snell's law of refraction as

$$[4] \qquad \frac{\sin\theta_1}{v_1} = \frac{\sin\theta_2}{v_2} = p$$

where θ_1 and θ_2 are the angles of incidence and refraction, respectively, v_1 and v_2 are the speeds of propagation in layers 1 and 2, respectively, and the quantity p is called the ray path parameter.

Fermat's principle states that a wave will take that ray path for which the travel time is stationary with respect to minor variations of the ray path. Chander (1977) utilizes Fermat's principle in deriving the governing equations that allow for seismic ray tracing from the source to the receiver. The following brief description for three-dimensional ray tracing through arbitrarily dipping interfaces in the velocity model is given in detail by Chander. In Fig. 5, V_1 to V_{n+1} represent the consecutive vertices of the seismic ray as it travels from the source to the SCPT receiver. V_1 identifies the source Cartesian coordinates (x_1, y_1, z_1) while V_{n+1} identifies the SCPT receiver Cartesian coordinates (x_{n+1}, y_{n+1}, z_{n+1}). It is required to trace the ray by determining the Cartesian coordinates of the vertices V_2 to V_n by implementing Fermat's principle and with the following data specified:

(1) The initial source and receiver Cartesian coordinates.

(2) The Cartesian plane interface equations where the vertices V_2 to V_n lie

$$[5] \qquad A_i x + B_i y + C_i z + D_i = 0 \qquad i = 2, \ldots, n$$

where the parameters A_i, B_i, and C_i define the normal to the interface plane and parameter D_i is derived by specifying a point on the plane.

(3) The interval velocities, v_i, $i = 2, .., n + 1$. This numbering convention for the algorithm implementation is subtly different from that illustrated in Fig. 5 so that it is easier to define and implement the necessary ray tracing governing equations. In the governing equations to follow, v_i is the constant velocity between interfaces $i - 1$ and i, i.e., along the segment of the ray between vertices V_{i-1} and V_i, v_2 is the velocity between the source and V_2, and v_{n+1} is the velocity between the SCPT receiver and vertex V_n.

Fig. 7. Solution space for tetrahedron simplex.

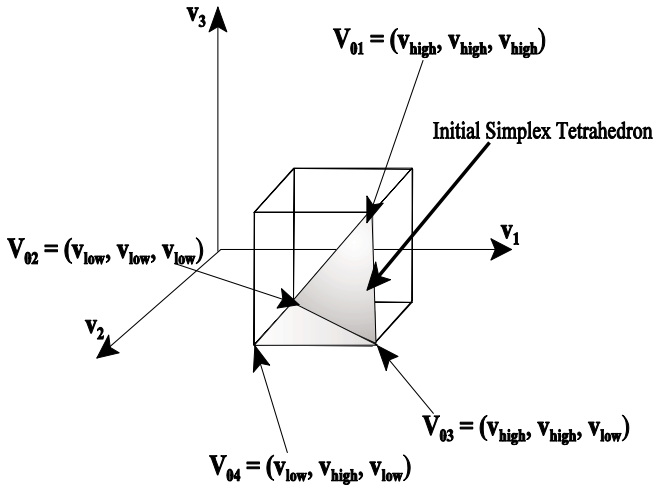

Chander's ray tracing governing equations

Fermat's principle of least time states that a wave will take the ray path for which the travel time is stationary with respect to minor variations of the ray path, that is, the change in travel time for an incremental change in ray path is zero (Sheriff and Geldart 1982). This principle leads to the condition that the ray path travels along the trajectory that requires minimum time between points. The travel time t along the ray V_1 to V_{n+1} is given by the sum

$$[6] \qquad t = \sum_{i=2}^{n+1} [(x_i - x_{i-1})^2 + (y_i - y_{i-1})^2 + (z_i - z_{i-1})^2]^{1/2} v_i^{-1}$$

Utilizing eq. [5], the travel time t may be expressed in terms of the x and y coordinates. To adhere to the requirement of Fermat's principle, the partial derivatives of t with respect to x_i and y_i are taken and set to zero as follows:

$$[7] \qquad \frac{\partial t}{\partial x_i} = \frac{x_i - x_{i-1} - A_i(z_i - z_{i-1})}{[(x_i - x_{i-1})^2 + (y_i - y_{i-1})^2 + (z_i - z_{i-1})^2]^{1/2} v_i} + \frac{x_i - x_{i+1} - A_i(z_i - z_{i+1})}{[(x_i - x_{i+1})^2 + (y_i - y_{i+1})^2 + (z_i - z_{i+1})^2]^{1/2} v_{i+1}} = 0 \qquad i = 2, \ldots, n$$

$$\frac{\partial t}{\partial y_i} = \frac{y_i - y_{i-1} - B_i(z_i - z_{i-1})}{[(x_i - x_{i-1})^2 + (y_i - y_{i-1})^2 + (z_i - z_{i-1})^2]^{1/2} v_i} + \frac{y_i - y_{i+1} - B_i(z_i - z_{i+1})}{[(x_i - x_{i+1})^2 + (y_i - y_{i+1})^2 + (z_i - z_{i+1})^2]^{1/2} v_{i+1}} = 0 \qquad i = 2, \ldots, n$$

The solution to the ray tracing problem is satisfied if the $2n - 2$ equations defined by eq. [7] hold simultaneously. Chander implements the multidimensional Newton-Raphson iteration technique to solve eq. [7]. The Newton-Raphson technique requires that initial vertices V_2 to V_n be specified that are iteratively updated so that eq. [7] holds. For the FMDSM, straight ray paths are assumed between source and receivers when specifying the initial vertices.

Fig. 8. FMDSM process flow diagram.

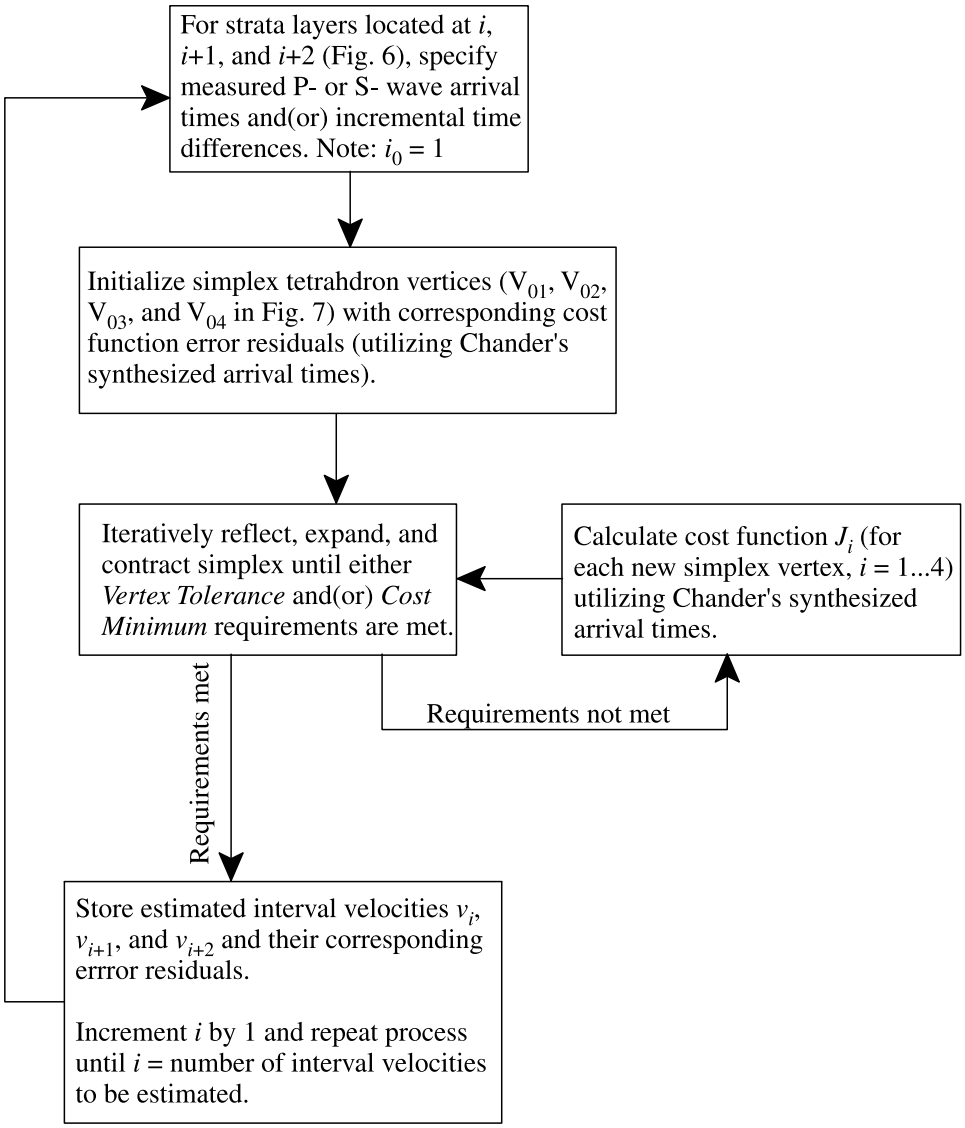

FMDSM proposed algorithm

The first step in implementing the FMDSM for deriving SCPT interval velocities is to specify the geometry of the stratigraphic profile under investigation. For example, in a typical SCPT the seismic cone data is acquired at depth intervals of 0.5–1 m as illustrated in Fig. 6. In Fig. 6 seismic data is obtained at 1 m intervals starting at 0.5 m down to a depth of 9.5 m resulting in a total of ten measurements. It is possible to have a greater amount of seismic data available within the profile estimated, but for simplicity one trace is assumed for each metre SCPT probe increment. The problem is to estimate the stratigraphic velocity intervals v_1 to v_{10} based upon the available seismic data. The Cartesian plane interfaces defined by eq. [5] have normals pointing along the z axis and are defined as $A_i = 0$, $B_i = 0$, $C_i = 1$, for $i = 0$–9. D_i is defined as the depth of the interface so that $D_i = 0, 1, \ldots, 9$, for $i = 0$–9, respectively.

The FMDSM recursively estimates the stratigraphic velocity intervals from v_1 to v_n by deriving three independent velocity estimates for each iteration. When the algorithm is running, the first three stratigraphic interval velocities are estimated (i.e., v_1, v_2, v_3), then the stratigraphic interval is incremented by one and interval velocities v_2, v_3, and v_4 are estimated. This process is repeated until the last stratigraphic interval velocity to be estimated is reached. This algorithm implies that estimates of interval velocity v_i for $i \geq 3$ will be determined three times (e.g., (v_1, v_2, v_3), (v_2, v_3, v_4), (v_3, v_4, v_5)) utilizing measurements acquired at five corresponding depth increments (e.g., v_1, v_2, v_3, v_4, v_5).

Once the geometry of the stratigraphic profile under investigations has been specified, the FMDSM implements the following steps:

(1) Specify vertices of initial tetrahedron. The FMDSM has a three-dimensional space defined as the possible values for the v_1, v_2, and v_3 interval velocities to be estimated. The interval velocities have the desirable property of being confined in the first quadrant of v_1–v_2–v_3 space (i.e., $v_1 > 0$, $v_2 > 0$, and $v_3 > 0$). In addition, we are assured that the interval P- and S-wave velocities lie in with certain minimum and maximum values; therefore the initial tetrahedron is specified so that it occupies a good portion of the solution space. The

Fig. 9. Specification of a ten layer variable velocity interval stratigraphic profile for testing the performance of the FMDSM.

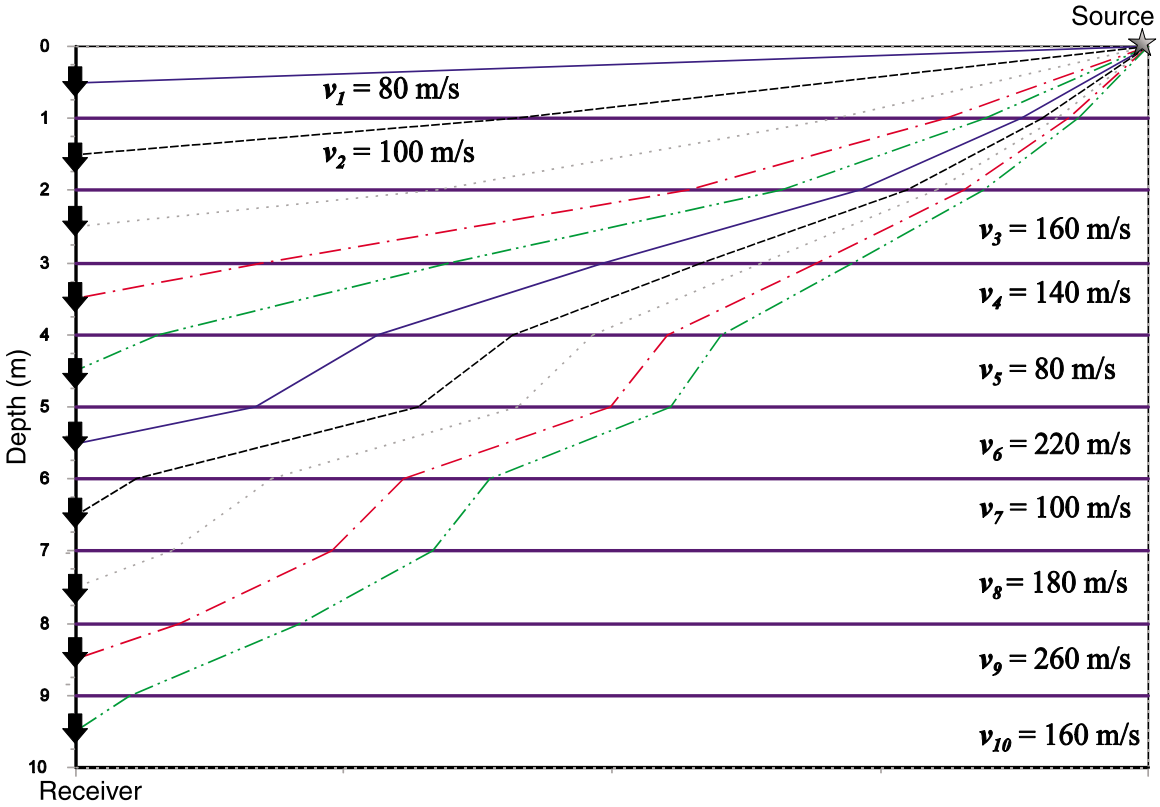

Fig. 10. Specification of a seven layer variable velocity interval stratigraphic profile for comparing the performance of the FMDSM with the standard straight ray interval velocity estimate.

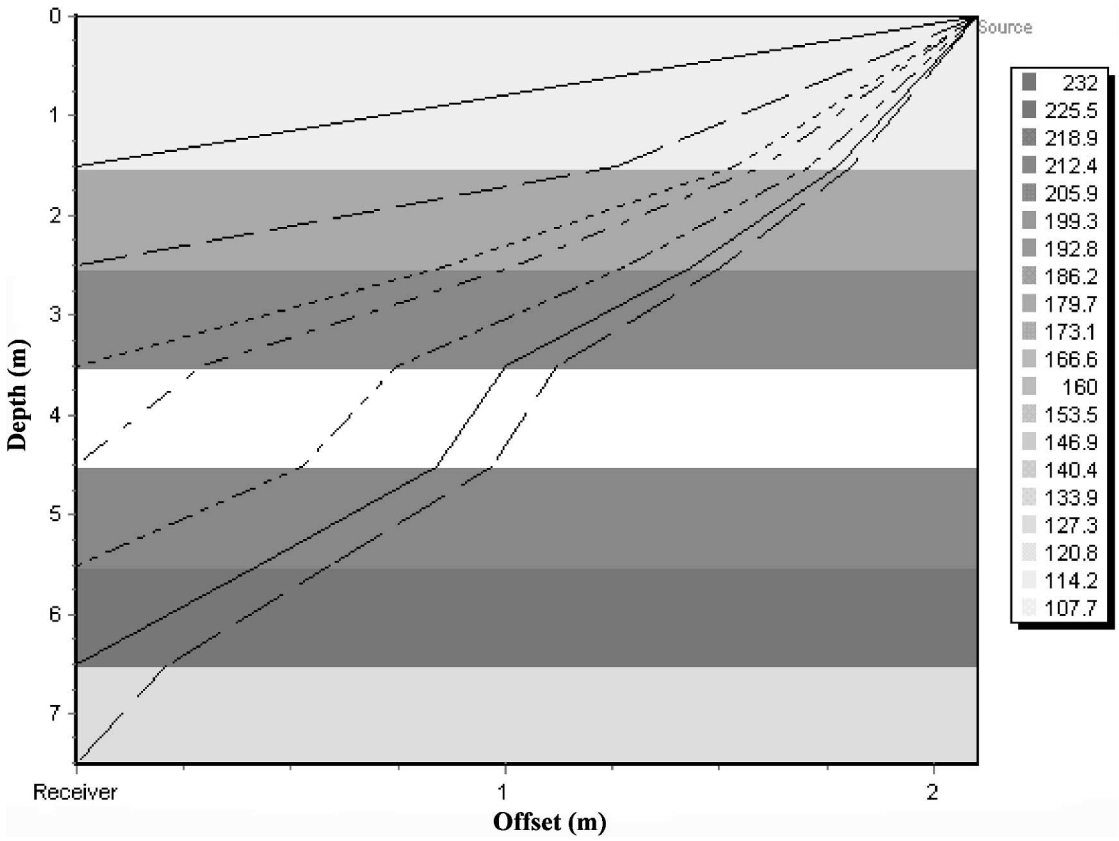

Fig. 11. Three layer stratigraphic profile.

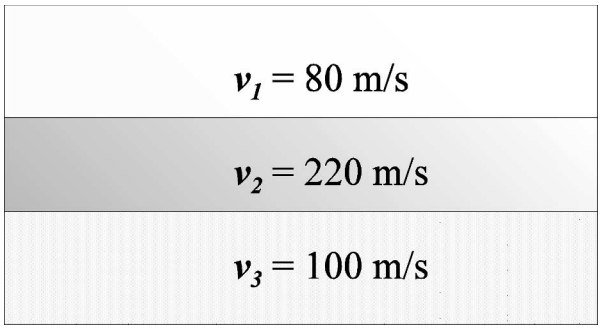

cube illustrated in Fig. 7 shows the solution space cube for the v_1–v_2–v_3 coordinate system where v_{high} and v_{low} define the possible maximum and minimum interval velocities, respectively, for the wavelet under study (i.e., P- or S-wave).

The FMDSM algorithm is very robust and obtains an optimal solution for very generic specifications of v_{high} and v_{low}. For example, setting v_{high} equal to the maximum possible shear or compression wave velocity in unconsolidated soils and v_{low} equal to zero is sufficient. The initial simplex tetrahedron illustrated in Fig. 7 has the following vertices specified:

$V_{01} = (v_{high}, v_{high}, v_{high})$, $V_{02} = (v_{low}, v_{low}, v_{low})$, $V_{03} = (v_{high}, v_{high}, v_{low})$, and $V_{04} = (v_{low}, v_{high}, v_{low})$.

(2) Utilizing forward modeling with Chander's ray tracing technique, synthesize measurements (e.g., P-, S-wave arrival times, incremental relative arrival times, incident angles, and P-, S-wave arrival time separations). Derive scalar cost function value based upon weighted least squares at each initial vertex.

(3) Implement previously outlined DSM steps (3)–(7).

(4) Repeat steps (1)–(3) until all interval velocities have been estimated.

Figure 8 illustrates a process flow diagram of the FMDSM.

FMDSM performance evaluation

As is standard practice in new mathematical algorithm designs, the previously outlined FMDSM formulation was extensively evaluated by processing synthetic data. Figure 9 illustrates a ten layer stratigraphic profile with varying interval velocities. Low and high medium velocities have been introduced within the profile so that there is significant seismic wave refraction and the forward modeling portion of the FMDSM could be assessed. The FMDSM parameters set for this test case were v_{high} = 600 m/s, v_{low} = 0 m/s, *VertexTolerance* = 1.0×10^{-8}, and *CostMinimum* = 1.0×10^{-8}. The variables *VertexTolerance* and *CostMinimum* were previously defined in items (6) and (7) of the DSM outline.

After synthesizing seismic wave arrival times based upon the stratigraphic profile illustrated in Fig. 9, the arrival times were fed into the FMDSM, and subsequent interval velocities and ray paths were estimated. The FMDSM exactly recovered the true interval velocities and provided the source receiver ray paths illustrated in Fig. 9. Upon close examination, it is found that the estimated ray paths adhered to Snell's law at the interface boundaries.

The ability of the FMDSM to improve upon the straight ray interval velocity estimate depends on several SCPT site parameters such as seismic cone – source offset, depth of interval velocity estimate, and variability of the in situ velocity profile to be estimated. Figure 10 illustrates a simulated SCPT were the seismic source is radially offset from the seismic probe by 2.1 m, the seismic data capture starts at 1.5 m and goes to a depth of 7.5 m at 1 m intervals.

Table 1 outlines the variable interval velocities and the interval velocity estimates from the FMDSM with comparisons made to the industry standard of assuming straight ray seismic wave propagation. An example of the calculation of the straight ray propagation interval velocity estimate is illustrated in Fig. 6 where $v_2 = (d_2 - d_1)/(t_2 - t_1)$. As shown in Table 1, the FMDSM exactly recovered the true interval velocities and provided the source receiver ray paths illustrated in Fig. 10. The straight ray interval velocity estimates did a poor job in estimating the true interval velocity estimates because the site parameters specified were not conducive to a straight ray assumption defined by $v_i = (d_i - d_{i-1})/(t_i - t_{i-1})$.

If there is not significant ray path refraction present in a seismic cone profile, the FMDSM may also be utilized to determine variable interval velocities for the same time series information. For example, if we are interested in 1 m increment interval velocities starting at a depth of 1.5 m for the traces illustrated in Fig. 9, we obtain the interval velocities illustrated in Table 2. This feature may be of use when correlating SCPT results with other types of in situ measurements.

The FMDSM was next tested for its ability to estimate an interval velocity when no measurement data (e.g., arrival time) for the stratigraphic layer under study is available. This leads to an underdetermined situation where we have more unknowns (e.g., interval velocities) than knowns (i.e., arrival time measurements). For example, consider the stratigraphic profile illustrated in Fig. 11. The interval velocities v_1, v_2, and, v_3 are estimated when only two interval measurements t_1 and t_2 are available. Table 3 shows the possible measurement combinations for the layers shown in Fig. 11 when only two measurements are available.

In Table 3, test case 1 results in a situation where there are several combinations of v_1, v_2, and v_3 that would give low or zero residual errors for the t_1 and t_2 measurements at layers 1, 2, and 3. In test case 2, we would obtain an accurate v_1 estimate, but again there would be several different combinations (e.g., average (i.e., $v_2 = v_3$), v_2 low and v_3 high, or v_2 low and v_3 high) of v_2 and v_3 to give a low error residual for the t_2 measurement. Test case 3 results in the situation where we have accurate estimates for v_1 and v_2, but nonsensical estimates for v_3 because there are no measurements available in this layer so that an error residual can be calculated.

As an example of the above analysis, consider the case where we have interval velocities v_1 = 80 m/s, v_2 = 220 m/s, and v_3 = 100 m/s. Table 4 illustrates the FMDSM estimation results when two measurement arrival times have been synthesized for test cases 1 to 3 in Table 3. As is illustrated in Table 4, we have averaged estimates for v_1, v_2, and v_3 for test case 1. In test case 2, the FMDSM gives an accurate estimate for v_1 and approximate estimates for v_2 and v_3. In test

Table 1. Comparing interval velocities (rounded off to the nearest integer) derived from the FMDSM and those obtained from the straight ray assumption.

Interval depth (m)	Arrival time (ms)	True interval velocities (m/s)	FMDSM interval velocity estimate (m/s)	Straight ray interval velocity estimate (m/s)
0–1.5	22.9795	112	112	112
1.5–2.5	24.2555	181	181	536
2.5–3.5	27.3112	209	209	267
3.5–4.5	36.96	101	101	94
4.5–5.5	40.7033	214	214	246
5.5–6.5	44.537	232	232	246
6.5–7.5	55.12	128	128	126

Table 2. Interval velocity (rounded off to the nearest integer) estimates from the FMDSM for a 0.5 m interval offset.

Interval depth (m)	FMDSM estimate (m/s)
0–1.5	86
1.5–2.5	124
2.5–3.5	149
3.5–4.5	102
4.5–5.5	118
5.5–6.5	138
6.5–7.5	128
7.5–8.5	213
8.5–9.5	198

Table 3. Possible measurement combinations for the underdetermined estimation problem.

Case	v_1	v_2	v_3
1	NA	A	A
2	A	NA	A
3	A	A	NA

Note: The letter A indicates that a measurement is available for the identified interval velocity, while NA denotes that no measurements are available for the associated interval velocity.

case 3, we have accurate estimates for v_1 and v_2, but a nonsensical estimate for v_3.

To constrain v_1 and v_3 (i.e., assume known) and utilize arrival time measurements at layers 1 and 3, the estimation problem is no longer underdetermined and an accurate estimate for v_2 can be made. The approach in the FMDSM for deriving an interval velocity from a layer where no measurement data is available is outlined as follows:

(1) Process available measurements and obtain accurate interval velocity estimates for layers where measurement data is available.

(2) Constrain medium velocities of boundary layers of interval v_{noData} that do not have measurements available.

(3) Use the measurements available at boundary layers and obtain an interval velocity estimate for v_{noData}.

The performance of the above steps (1)–(3) is demonstrated by reprocessing the profile illustrated in Fig. 9. To simulate the effect of no measurement data the measurement weight for the arrival time occurring in stratigraphic interval six of Fig. 9 is set to zero. In this test the modified FMDSM algorithm gives exact interval velocity estimates for the layer that has arrival time measurement data available. The estimate for layer six in this first run is 202 m/s instead of 220 m/s. The FMDSM algorithm is again executed with the above steps (1)–(3) implemented. In this case, the algorithm gives the exact interval estimate of 220 m/s.

Table 4. FMDSM estimation results for the cases outlined in Table 3.

Case	v_1	v_2	v_3
1	105	108	104
2	80	212	104
3	80	220	67

It is not required to constraint the boundary interval velocities if greater measurement information were available, such as source wavelet incident angles derived from biaxial or triaxial SCPT probes. In this case, the calculated cost function is sufficiently constrained that a unique velocity estimate can be obtained at a stratigraphic layer where measurement data is not available.

Conclusions

Seismic cone penetration testing is a very valuable geotechnical tool in obtaining vertical profiles of P- and S-wave velocities that are directly related to the elastic properties of soil. SCPT is a desirable methodology for obtaining in situ seismic velocities due to the excellent sensor and soil coupling and simplicity of source wavelet generation. The accurate determination of P- and S-wave velocities from the recorded seismic cone time series is of paramount importance to the evaluation of reliable elastic constants. Furthermore, since the shear and compression wave velocities are squared in deriving the elastic constants, small variations in the estimated velocities can cause appreciable errors. This paper presented an algorithm, FMDSM, that offered several advantages over conventional estimation techniques when deriving SCPT interval velocity profiles.

Some of the benefits over conventional techniques provided by the FMDSM consist of utilization of Snell's law at layer boundaries for ray path refraction; optimization of a nonlinear cost function that takes into account more detail of the SCPT testing environment and subsequent seismic data recorded compared to standard techniques; allowance for measurement weights to be specified; the possibility to incorporate unlimited input data (e.g., crossover point arrival

times, maximum crosscorrelation time shifts, angles of incidence, and P-, S-wave time separations) into the interval velocity estimation algorithm; the ability to accurately interpolate interval velocities when measurement data is not available; and it provides meaningful error residuals that indicate the accuracy of the estimated interval velocity.

The performance of the FMDSM is assessed by processing synthesized data, where very encouraging results are obtained. The ability of the FMDSM to improve upon the straight ray interval velocity estimate depends on several SCPT site parameters such as seismic cone – source offset, depth of interval velocity estimate, and variability of the in situ velocity to be estimated. It has been demonstrated that depending upon the values of the previously described variables, the FMDSM can provide substantially more accurate interval velocity estimates than the straight ray assumption, and the FMDSM may also be utilized to determine variable interval velocity estimates so that comparisons or correlations can be made with other types of in situ measurements.

References

Andrus, R.D., Stokoe, K.H., and Chung, R.M. 1999. Draft guidelines for evaluating liquefaction resistance using shear wave velocity measurements and simplified procedures. NISTIR 6277. National Institute of Standards and Technology, Gaithersburg, Md.

Baziw, E.J. 1993*a*. Digital filtering techniques for interpreting seismic cone data. Journal of Geotechnical Engineering, ASCE, **119**(6): 98–1018.

Baziw, E.J. 1993*b*. Method for determining velocity and confidence levels of acoustic waves in penetrable ground. U.S. Patent 5 177 709. (Canadian Patent 2 077 387-1; 1996).

Baziw, E.J., and Weir-Jones, I. 2002. Application of Kalman filtering techniques for microseismic event detection. Pure and Applied Geophysics, **159**: 449–473.

Baziw, E.J., Campanella, R.G., and Sully, J.P. 1989. Interpretation of seismic cone data using digital filtering techniques. *In* Proceedings of the 12th International Conference on Soil Mechanics and Foundation Engineering, Rio de Janeiro, 13–18 Aug. 1989. A.A. Balkema, Rotterdam.

Baziw, E.J., Tichy, J. and de Caprona, G. 2000. Data acquisition in seismic cone penetration testing. *In* Proceedings of the 3rd International Symposium on Integrated Technical Approaches to Site Characterization (ITASCE), Argonne, IL, 11–14 Sept. 2000. Argonne National Laboratory. pp. 69–72.

Campanella, R.G., Robertson, F.T.C., and Gillespie, D. 1986. Seismic cone penetration test. *In* Proceedings of INSITU86. American Society of Civil Engineers (ASCE) Geotechnical Special Publication. No. 6, pp. 116–130.

Chander, R. 1977. On tracing seismic rays with specified end points in layers of constant velocity and plane interfaces. Geophysical Prospecting, **25**: 120–124.

Finn, W.D.L. 1984. Dynamic response analysis of soils in engineering practice. *In* Mechanics of engineering materials. John Wiley & Sons Ltd., New York. Chapter 13.

Gibowicz, S.J., and Kijko, A. 1994. An introduction to mining seismology; Vol. 55 in the international geophysics series, Academic Press. pp. 48–77.

Kanasewich, E.R. 1981. Time sequence analysis in geophysics. 3rd ed., The University of Alberta Press, Edmonton, AB. pp. 328–354.

Mooney, H.M. 1977. Handbook of engineering geophysics. BISON Instruments, Inc., Minneapolis, MN.

Nelder, J.A., and Mead, R. 1965. A simplex method for function optimization. Computing Journal, **7**: 308–313.

Sheriff, R.E., and Geldart, L.P. 1982. Exploration seismology, Vol. 1, 2nd ed., Cambridge University Press, Cambridge, U.K.

Vance, J.B., Hassani, F.P., and Mottahed, P. 1988. Improved determination of microseismic source location using a simplex technique. IEEE Transactions on Industry Applications, **24**(4): 666–671.